# SELF-SIMILAR PARTICLE SIZE DISTRIBUTIONS DURING COAGULATION AND SETTLING; THEORY AND EXPERIMENTAL VERIFICATION



James R. Hunt[1]
W. M. Keck Laboratory of Environmental Engineering Science
California Institute of Technology
Pasadena, California 91125

October 15, 1980

[1]Present address: Division of Sanitary, Environmental, Coastal, and Hydraulic Engineering, University of California, Berkeley, California 94720.

Abstract

A quantitative theory for particle coagulation and settling in continuous particle size distributions is presented. The analysis assumes a local equilibrium in the size distribution maintained by a particle flux through the size distribution. Only partical collisions caused by Brownian motion, fluid shear, and differences in settling velocities are considered. For intervals of particle size where only one coagulation or settling mechanism is dominant, dimensional analysis predicts self-similar size distributions which contain only one dimensionless constant for each mechanism. Experiments were designed to test these predictions with clay particles in artificial seawater sheared in the gap between concentric rotating cylinders. Particle size distributions measured over time were self-similar in shape and agreed with the Brownian and shear coagulation predictions in terms of shape and dependence on fluid shear rate and particle volume flux through the size distribution.

In many industrial processes particle removal from fluids is important because,either the particles contain important minerals which are being concentrated, or the particles are pollutants which must be removed before effluent discharge. The particles of interest are typically very small and can not be separated over reasonable time periods by quiescent settling. To accelerate suspended particle removal, particles are coagulated or aggregated into larger particles which have greater settling velocities and can be separated from the fluid in reasonable time periods. Particle coagulation is also important in controlling the removal of suspended particles from natural waters, especially estuaries and coastal waters.

A fundamental understanding of particle coagulation has been limited to the initial coagulation kinetics of particles uniform in size. These results can not be applied quantitatively to suspensions containing continuous distributions of particle sizes as are commonly encountered. Because of the lack of a verified theory for coagulation in continuous particle size distributions, design of particle separation systems involving coagulation and settling has been empirical and dependent on extensive pilot plant studies. This paper presents a theoretical derivation of coagulating and settling particle size distributions extending results obtained earlier by Friedlander (1960a,b). The approach, valid after sufficient time, assumes the particle size distribution is in local equilibrium maintained by a flux of particles through the size distribution. The size distribution predictions for Brownian and shear coagulation are experimentally verified with clay particles in artificial seawater.

## 1. Coagulation and Sedimentation Mechanisms

A continuous distribution of particle sizes is represented by two size distribution functions, $n(d_p)$ distributed on particle diameter, $d_p$, and $n(m)$ distributed on particle mass, $m = \rho_p \frac{\pi}{6} d_p^3$, where $\rho_p$ is the particle density. The number of particles, dN, in a small interval of diameter, $d(d_p)$, and a corresponding interval of mass, dm, is given by

$$dN = n(d_p)\, d(d_p) = n(m)dm \quad . \tag{1.1}$$

Particle size distributions in terms of mass are convenient for the theoretical derivation since mass is conserved during coagulation. For experimental measurement, particle size distributions in terms of diameter are more convenient. The transformation between the two distributions is given by

$$n(m) = \frac{d(d_p)}{dm}\, n(d_p) = \frac{2}{\pi \rho_p} d_p^{-2}\, n(d_p) \quad . \tag{1.2}$$

The dimensions of $n(m)$ are number of particles per volume of fluid per particle mass, represented as $[L^{-3}M^{-1}]$ where [L] is a fluid length unit and [M] is a particle mass unit.

A general equation describing a particle size distribution undergoing coagulation and settling is

$$\frac{\partial n(m)}{\partial t} = \frac{1}{2}\int_0^m \beta'(\bar{m},m-\bar{m})\, n(\bar{m})\, n(m-\bar{m})\, d\bar{m}$$

$$- \int_0^\infty \beta'(m,\bar{m})\, n(m)\, n(\bar{m})\, d\bar{m}$$

$$- \frac{g(\rho_p-\rho_f)}{18\,\mu}\left(\frac{6}{\pi\rho_p}\right)^{2/3} m^{2/3}\,\frac{\partial n(m)}{\partial z} \qquad (1.3)$$

where the dependence of the size distribution on vertical position, z, positive downward and time, t, were not indicated explicitly. In Equation (1.3) the first term on the right hand side represents the collision of particles producing a particle of mass m, where $\beta'(\bar{m},m-\bar{m})$ is a collision function for particles of mass $\bar{m}$ colliding with particles of mass $m-\bar{m}$ by all coagulation mechanisms. The second term is the removal of particles of mass m by coagulation with all particles. Particle removal by settling using Stokes' equation is represented by the third term where g is the gravitational acceleration, $\mu$, the fluid viscosity, and $\rho_f$, the fluid density.

In this study three coagulation mechanisms are considered, each with a collision function represented below for collisions between particles of diameters $d_i$ and $d_j$ and equivalently with masses $m_i$ and $m_j$. For collisions arising from the Brownian or thermal motion of particles Smoluchowski (1917) showed that

$$\beta_b(d_i,d_j) = \frac{2kT}{3\,\mu}\,\frac{(d_i+d_j)^2}{d_i d_j} \qquad (1.4)$$

$$\beta'_b(m_i,m_j) = \frac{2kT}{3\mu}\,\frac{(m_i^{1/3}+m_j^{1/3})^2}{m_i^{1/3}\,m_j^{1/3}} \qquad (1.5)$$

where k is the Boltzmann constant, and T, absolute temperature. In transforming Equation (1.4) into (1.5), particle density was assumed to be independent of particle size. If a fluid is sheared in either laminar or turbulent flow, particles moving with the fluid collide, and the collision functions for shear coagulation are, as also shown by Smoluchowski (1917),

$$\beta_{sh}(d_i,d_j) = \frac{G}{6}(d_i + d_j)^3 \tag{1.6}$$

$$\beta_{sh}(m_i,m_j) = \frac{G}{\pi\rho_p}(m_i^{1/3} + m_j^{1/3})^3 \tag{1.7}$$

where G is the fluid shear rate or mean velocity gradient.

Smoluchowski arrived at the Brownian and shear coagulation collision functions assuming geometrical collisions unhindered by hydrodynamic, electrostatic, or van der Waals forces during collision (see Friedlander, 1977). Corrections for these forces have been obtained when spheres of equal size collide by Brownian motion (Spielman, 1970; Honig et al., 1971) and by fluid shear (van de Ven and Mason, 1977; Zeichner and Schowalter, 1977). For collision of spheres of unequal size, predictions are not available. The experimental data of Manley and Mason (1955) indicate that hydrodynamic forces greatly limit shear induced collisions when the colliding particles differ by a factor of two or more in diameter.

The third coagulation mechanism considered is when a faster settling particle overtakes and collides with a slower settling particle. The collision function for differential sedimentation coagulation is the collision cross section times the difference in particle Stokes' settling

velocities, assuming a constant particle density

$$\beta_{ds}(d_i,d_j) = \frac{\pi g(\rho_p-\rho_f)}{72\,\mu}\ (d_i+d_j)^2\ \left|d_i^2-d_j^2\right| \tag{1.8}$$

$$\beta_{ds}(m_i,m_j) = \left(\frac{6}{\pi}\right)^{4/3}\frac{\pi g(\rho_p-\rho_f)}{72\,\mu}\ \rho_p^{-4/3}\ (m_i^{1/3}+m_j^{1/3})^2\ \left|m_i^{2/3}-m_j^{2/3}\right| \tag{1.9}$$

Hydrodynamic forces are known to limit the collision efficiency of this mechanism for water droplets in air (Mason, 1971), but corrections for hydrodynamic, electrostatic, and van der Waals forces are not available for particles suspended in water. In the collection of particles on filter media, these forces are important in determining the collection efficiency (Spielman, 1977).

## 2. Previous Solutions for Coagulation and Sedimentation

This section reviews the analytical and numerical solutions obtained previously for Equation (1.3). There are two general types of solutions, either all particles are taken as initially equal in size, that is, monodisperse, or a size distribution of particles is considered.

For a monodisperse suspension, coagulation kinetics are straightforward if settling is neglected. If coagulation is by Brownian motion only, Equation (1.3) becomes

$$\frac{dN}{dt} = - \frac{4kT}{3\mu} N^2 \tag{2.1}$$

where N is the total particle concentration. For an initial particle concentration of $N_o$, Equation (2.1) has the solution

$$N(t) = \frac{N_o}{1 + \frac{4kT}{3\mu} N_o t} \quad . \tag{2.2}$$

This solution is valid only for times less than the half-time of the reaction, $3\mu/4kTN_o$, since Equation (2.1) assumes only particles of equal size collide. Experimentally observed coagulation rates were less than the theoretical rate with the discrepancy explained by the influence of hydrodynamic and van der Waals forces (Lichtenbelt et al., 1974). Experiments were conducted in solutions of high ionic strength which eliminated electrostatic forces between particles.

In a monodisperse, non-settling suspension dominated by shear coagulation, Equation (1.3) reduces to

$$\frac{dN}{dt} = -\frac{2}{3} G d_p^3 N^2 \qquad (2.3)$$

and noting that total suspended particle volume, $V = \frac{\pi}{6} d_p^3 N$, is conserved, then

$$\frac{dN}{dt} = -\frac{4}{\pi} VGN \quad . \qquad (2.4)$$

The solution to Equation (2.4) is

$$N(t) = N_o \exp(-\frac{4}{\pi} VGt) \qquad (2.5)$$

which is valid only for the initial coagulation period $t < \pi/4VG$. The first order rate expression has been verified by Swift and Friedlander (1964) in laminar shear flow and by Birkner and Morgan (1968) in turbulent flow. Again, corrections for hydrodynamic and van der Waals forces explained the difference between observed and theoretical rates (van de Ven and Mason, 1977; Zeichner and Schowalter, 1977). In a monodisperse suspension, differential sedimentation coagulation is not expected to occur because $\beta(d_i,d_i) = 0$.

These solutions of Equation (1.3) for monodisperse suspensions are not applicable for the analysis of coagulation in suspensions containing

a broad distribution of particle sizes. There have been two approaches to solving Equation (1.3) for a continuous particle size distribution, using either direct numerical solutions or asymptotic solutions for later times by a self-preserving transformation. Two recent examples of direct numerical solutions are Gelbard and Seinfeld (1979) for aerosol dynamics and Lawler et al. (in press) for hydrosol dynamics. These numerical solutions have not been verified with experimental data.

Partial solutions to Equation (1.3) have been obtained by self-preserving transformations. Friedlander (1960a,b) showed that a self-preserving transformation reduced the equation for Brownian coagulation and settling from a partial integro-differential equation to an ordinary integro-differential equation. The general shear coagulation equation also had a self-preserving transformation and experimentally measured size distributions of coagulating hydrosols and emulsions approached a self-preserving distribution after sufficient time (Swift and Friedlander, 1964). A self-preserving transformation also existed for simultaneous Brownian and shear coagulation only if the shear rate over time was proportional to the total number of particles (Wang and Friedlander, 1967). Pulvermacher and Ruckenstein (1974) and Drake (1976) have discussed the existence of self-preserving solutions for a number of coagulation mechanisms.

The concept of a self-preserving transformation of Equation (1.3) has had considerable utility in aerosol coagulation studies, but the application to hydrosols is limited. For aerosols, Brownian coagulation is usually the dominant mechanism for larger aerosol growth, while for hydrosols, Brownian and shear coagulation are known to be important and possibly coagulation by differential sedimentation. Thus, for hydrosols, all

coagulation mechanisms must be considered and the restriction necessary for a self-preserving transformation that the shear rate is proportional to the particle concentration, is not a general result with wide application. Quantitative application of the self-preserving transformation also requires corrections to the collision functions for hydrodynamic, electrostatic, and van der Waals forces.

## 3. Self-Similar Solutions for Coagulation and Settling

A general solution to Equation (1.3) will not be attempted, instead self-similar solutions are obtained dimensionally after considerable simplification. The approach is a modification of Friedlander (1960a,b) where Brownian coagulation and settling of atmospheric aerosols were considered. Friedlander's analysis is directly analogous to previous work on the universal equilibrium spectra of turbulent variations in velocity and scalar fields (Batchelor, 1953, 1959).

Four major assumptions are required in the analysis of coagulating and settling particle distributions. The first, and major, limiting assumption is that the particle distribution is in a dynamic steady state, or equilibrium. There is an assumed source of small particles which coagulate through the size distribution to an aggregate size large enough for removal by settling. For a small interval of particle size there is a balance between the particle mass coagulating into that interval and the mass lost from the interval by coagulation or settling. The existence of a dynamic steady state distribution maintained by a mass flux through the distribution limits the application of the results to long times after the start of particle coagulation. The mass flux is denoted by $\rho_p E$ with dimensions

$[ML^{-3}t^{-1}]$ where E is the volume flux and [t] is the time unit.

The second assumption is that only one coagulation or settling mechanism is dominant at a given particle size. To show the strict validity of this assumption would require demonstrating that, the contribution to the mass flux at a given particle size is dominated by particle collisions near that size, and also, that only one mechanism is significant at that size. The coagulation collision functions given in Equations (1.4) through (1.9) imply that collisions are possible between particles of all sizes if various fluid and particle forces are not considered. For Brownian coagulation, the influence of hydrodynamic forces on the collision of unequal spheres could be obtained following Spielman (1970), but no calculations or data are available to estimate the influence of hydrodynamic forces on hindering the collision between unequal spheres. For shear and differential sedimentation coagulation hydrodynamic forces probably hinder collision between particles different in size. Based on the limited information, collisions between particles much different in size can be assumed to have little contribution to the mass flux through the distribution.

Considering collisions only between particles comparable in size, regions exist where only one coagulation mechanism is dominant. In Figure 1 the coagulation collision functions in Equations (1.4), (1.6), and (1.8) are plotted for particles of size $d_p$ colliding with particles of size $\frac{1}{2} d_p$ for reasonable values of temperature, fluid shear rate, and particle density. Under these conditions, collisions of a particle and

and another one-half its diameter occur most frequently by Brownian motion for $d_p < 1$ μm, shear coagulation causes the greatest number of collisions for 2 to 60 μm particles, and for $d_p > 100$ μm, differential sedimentation coagulation is the dominant collision mechanism. Other choices of the ratio of colliding particle diameters, fluid shear rates, and particle density would shift the curves but still retain the regions of dominance; Brownian at smallest diameters, shear at intermediate sizes, and differential sedimentation coagulation at larger diameters. Particle removal by gravitational settling can not be compared with the coagulation mechanisms in this plot, but it is reasonable that gravitational settling is dominant for the largest particles.

The third assumption is that the efficiency of particle sticking on collision is independent of particle size. Most particles suspended in water are charged, and electrostatic repulsive forces exist between particles. At sufficiently high concentration of ions in solution, the electrostatic forces are masked and attractive van der Waals forces cause the sticking of particles. Overbeek (1977) reviews current problems in understanding suspended particle stability at lower ionic strengths when electrostatic forces exist and collision efficiency may be a function of particle size.

The fourth assumption requires that the particle distribution depends only on six terms: (1) particle mass, (2) the flux of particle mass through the distribution, parameters representing (3) Brownian, (4) shear, and (5) differential sedimentation coagulation, and (6) a gravitational settling parameter. The coagulation and settling parameters and associated dimensions are obtained from the Equations (1.3), (1.5), (1.7) and (1.9),

and the parameters are chosen to be independent of particle mass:

Brownian

$$K = \frac{kT}{\mu} \qquad [L^3 t^{-1}] \tag{3.1}$$

shear

$$\rho_p^{-1} G \qquad [L^3 M^{-1} t^{-1}] \tag{3.2}$$

differential sedimentation

$$\rho_p^{-4/3} S = \rho_p^{-4/3} \frac{g(\rho_p - \rho_f)}{\mu} \qquad [L^3 M^{-4/3} t^{-1}] \tag{3.3}$$

settling

$$\rho_p^{-2/3} S = \rho_p^{-2/3} \frac{g(\rho_p - \rho_f)}{\mu} \qquad [L M^{-2/3} t^{-1}] \; . \tag{3.4}$$

These parameters and the mass flux, $\rho_p E$, assume that particle density is independent of particle size. The advantage of separating out the particle density from the parameters will be clearer when n(m) predictions are transformed to $n(d_p)$.

With these assumptions the particle mass distribution has the following functional form

$$n = n(m, \rho_p E, K, \rho_p^{-1} G, \rho_p^{-4/3} S, \rho_p^{-2/3} S) \; . \tag{3.5}$$

Selecting an interval of particle mass where only Brownian coagulation is dominant, Equation (3.5) reduces to

$$n = n(m, \rho_p E, K) \tag{3.6}$$

which contains four variables (n,m,$\rho_p$E, and K) and three dimensions (M,L, and t). The prediction for a Brownian coagulation dominated distribution is obtained by dimensional arguments as

$$n(m) = A_b' \left(\frac{\rho_p E}{K}\right)^{1/2} m^{-3/2} \tag{3.7}$$

where $A_b'$ is a dimensionless constant. Similarly, predictions are obtained for intervals dominated by shear and differential sedimentation coagulation and gravitational settling as follows:

shear

$$n(m) = A_{sh}' \left(\frac{\rho_p E}{\rho_p^{-1} G}\right)^{1/2} m^{-2}, \tag{3.8}$$

differential sedimentation

$$n(m) = A_{ds}' \left(\frac{\rho_p E}{\rho_p^{-4/3} S}\right)^{1/2} m^{-13/6}, \tag{3.9}$$

and settling

$$n(m) = A_s' \left(\frac{\rho_p E}{\rho_p^{-2/3} S}\right)^{3/4} m^{-9/4}, \tag{3.10}$$

where $A_{sh}'$, $A_{ds}'$, and $A_s'$ are dimensionless constants.

As a practical matter it is particle size distributions, $n(d_p)$, which are measured rather than n(m), and so the transformation indicated in Equation (1.2) gives:

Brownian

$$n(d_p) = A_b \left(\frac{E}{K}\right)^{1/2} d_p^{-5/2} \tag{3.11}$$

shear

$$n(d_p) = A_{sh} \left(\frac{E}{G}\right)^{1/2} d_p^{-4} \tag{3.12}$$

differential sedimentation

$$n(d_p) = A_{ds} \left(\frac{E}{S}\right)^{1/2} d_p^{-9/2} \tag{3.13}$$

settling

$$n(d_p) = A_s \left(\frac{E}{S}\right)^{3/4} d_p^{-19/4} \tag{3.14}$$

where $A_b$, $A_{sh}$, $A_{ds}$, and $A_s$ are dimensionless constants different from those appearing in Equations (3.7) through (3.10). The analysis is in terms of n(m) because the assumptions are more apparent and the dimensional arguments are less ambiguous than a previous analysis in terms of $n(d_p)$ (Hunt, in press).

The predictions in Equations (3.11) through (3.14) are in reasonable agreement with particle size distributions observed in oceanic waters. These predictions also appear to account for the maximum in particle concentration that has been frequently observed in the oceanic thermocline as clearly there is a decreased rate of fluid shear in the thermocline (Hunt, in press).

## 4. Experimental Procedures for Testing Predictions

This section summarizes the experimental procedures for testing the Brownian and shear coagulation predictions. With the instrumentation available for measuring particle size distributions, larger aggregates could not be sized, and predictions for differential sedimentation coagulation and gravitational settling were not tested. Hunt (1980) contains a more complete description of experimental procedures.

### Data Presentation and Normalization

Number distributions, $n(d_p)$, are experimentally measured, but they are not the best representation of experimental data described by the Brownian and shear coagulation predictions in Equations (3.11) and (3.12). One convenient form for representation of size distribution data is a volume distribution, $dV/d(\log d_p)$, which is the suspended particle volume in a logarithmic interval of particle size, and is related to the number distribution by (see Friedlander, 1977)

$$\frac{dV}{d(\log d_p)} = \frac{2.3\pi}{6} d_p^4 n(d_p) \tag{4.1}$$

where 2.3 is ℓn 10. Predicted volume distributions for Brownian and shear coagulation become

Brownian

$$\frac{dV}{d(\log d_p)} = \frac{2.3\pi}{6} A_b \left(\frac{E}{K}\right)^{1/2} d_p^{3/2} \tag{4.2}$$

shear

$$\frac{dV}{d(\log d_p)} = \frac{2.3\pi}{6} A_{sh} \left(\frac{E}{G}\right)^{1/2} \quad . \tag{4.3}$$

Experiments were designed to test the dependence of the volume distribution on particle diameter, particle volume flux, E, and fluid shear rate, G. A convenient way to present the data and to test the agreement with predictions is to normalize or scale the data such that all volume distributions are represented by a single distribution. Particle diameters are normalized by the characteristic diameter which separates Brownian coagulation dominance from shear coagulation dominance. The particle diameter where Brownian and shear coagulation have equal collision frequency is found by equating Equations (1.4) and (1.6) for $d_i = d_j$, giving a particle diameter of $(2kT/\mu G)^{1/3}$ or $(2K/G)^{1/3}$. A normalized particle diameter, $\delta$, is defined as

$$\delta = d_p \left(\frac{G}{K}\right)^{1/3} \tag{4.4}$$

with the property that Brownian coagulation is expected to be dominant for $\delta << 2^{1/3}$ and shear coagulation for $\delta >> 2^{1/3}$. The normalized diameter is proportional to the cube root of a Péclet number, $Pe = Gd_p^2/D$, where $D = kT/3\pi\mu d_p$, the Stokes-Einstein expression for particle diffusivity. The Péclet number is the ratio of fluid shear particle mass transport to diffusive mass transport.

The normalized volume distribution, $d\bar{V}/d(\log \delta)$, is taken as

$$\frac{d\bar{V}}{d(\log \delta)} = \frac{dV}{d(\log d_p)} \left(\frac{G}{E}\right)^{1/2} \tag{4.5}$$

which,combined with Equation (4.4),transforms the Brownian and shear coagulation predictions into

Brownian

$$\frac{d\bar{V}}{d(\log\delta)} = \frac{2.3\pi}{6} A_b \delta^{3/2} \tag{4.6}$$

shear

$$\frac{d\bar{V}}{d(\log\delta)} = \frac{2.3\pi}{6} A_{sh} \cdot \tag{4.7}$$

With this normalization procedure, all experimental data in agreement with the Brownian and shear coagulation predictions should collapse onto a single curve described by Equation (4.6) for $\delta << 2^{1/3}$ and Equation (4.7) for $\delta >> 2^{1/3}$.

## Experimental Methods

This section describes the preparation of the aqueous and solid phases, the size distribution measurement technique, the method for controlling the fluid shear rate, and the procedure for determining the volume flux through the distribution. Experiments were conducted at room temperature (22-24°C) with low suspended particle volume concentration, fixing the value of the Brownian coagulation parameter, $K = kT/\mu = 4.38 \times 10^{-12}$ $cm^3$ $s^{-1}$.

All experiments were conducted in artificial seawater prepared according to a recipe of Lyman and Fleming from Riley and Skirrow (1965). Background suspended particles were removed from the artificial seawater by 0.22 μm Millipore filtration.

Clay minerals were selected for the testing of the predictions because of their presence in natural waters and the importance of clay particle surfaces in transporting adsorbed pollutants. The clays were obtained from Ward's Natural Science Establishment, Inc. and were representative of clay minerals previously characterized by the American Petroleum Institute (Kerr et al., 1949-50). Kaolinite (A.P.I. No. 4) was from Oneal Pit, Macon, Georgia, USA, and illite (A.P.I. No. 35) was from Fithian, Illinois, USA. Clay particles are not spherical but consist of negatively charged flat sheets with positively charged edges. Illite clay particles have a greater surface charge density than kaolinite particles because of a greater cation exchange capacity. Crushed clay particles were

cleaned and the clay surfaces were converted to their sodium form following procedures recommended by van Olphen (1977). The clay suspensions were allowed to settle quiescently to remove particles greater than 2 μm, equivalent spherical diameter. Edzwald et al. (1974) observed that the ionic strength of seawater was sufficient to destabilize clay particles.

Aggregate size distributions were measured with a Model ZBI Coulter Counter interfaced with a Nuclear Data logarithmic amplifier and multi-channel analyzer. The Coulter Counter counts and sizes aggregates by pulling aggregates, one at a time, through a small aperture and measuring the change in electrical resistance across the aperture. The resistance change is proportional to the particle volume and the instrument is able to count and size suspended particles.

To control the fluid shear rate, the suspension was sheared in the gap between two concentric rotating cylinders which gave a well defined mean shear rate with little variation about the mean. The apparatus was aligned vertically to remove larger aggregates by settling. With a fixed inner cylinder of 7.5 cm diameter and a gap width of 0.63 cm, shear rates of 1/2 $s^{-1}$ through 32 $s^{-1}$ were possible. Experimental evidence indicated that a fluid instability occured at 32 $s^{-1}$, probably caused by cylinder surface roughness. Taylor's (1936) experiments with a similar cylinder diameter and gap width developed instabilities at a shear rate of 250$s^{-1}$.

During batch experiments in laminar shear flow, the particle volume flux was obtained from the rate of change in total suspended volume, V(t),

$$E(t) \simeq - \frac{dV(t)}{dt} \quad . \tag{4.8}$$

The expression is only approximate as discussed below. In the Appendix the coagulation and settling size distribution predictions are integrated

to obtain the rate of change in total suspended volume which is second order in total suspended volume, viz.,

$$\frac{dV(t)}{dt} = - bV^2(t), \tag{4.9}$$

with a solution

$$V(t) = \frac{1}{a+bt}, \tag{4.10}$$

where a is a constant and b is a parameter dependent on the fluid shear rate. Substituting Equation (4.9) into Equation (4.8), gives the desired relationship for the instantaneous volume flux

$$E(t) = bV^2(t) \quad . \tag{4.11}$$

The value of b was obtained experimentally from the slope of an inverse volume plot with time, as in Equation (4.10). Equation (4.11) gives overestimates of the Brownian and shear coagulation volume flux in batch experiments because, as the total suspended volume decreases, settling dominance shifts to smaller diameters. This shift in settling dominance causes a loss of suspended volume from the distribution at larger diameters which contributes to the volume flux, but it is not part of the volume flux experienced by Brownian and shear coagulation.

During aggregate counting and sizing, larger aggregates were broken up and the total suspended volume could not be obtained from the measured particle size distribution. Total suspended volume was determined from

suspension optical absorbance, which is a measure of the light scattered by the suspended particles. Absorbance of a shaken suspension at low concentration was proportional to total suspended volume. Absorbance measurements were made with a 1 cm or a 5 cm optical cell, depending on the suspension concentration.

An experiment was started by rapidly mixing 2 mL of concentrated clay suspension with 200 mL of filtered artificial seawater in a 250 mL beaker. The destabilized particle suspension was poured into the gap of the rotating cylinder apparatus, and after 10 to 25 minutes of shearing, the first sample was withdrawn for analysis. Analysis included measurement of particle size distribution and determination of total suspended volume from suspension absorbance. Samples were withdrawn one to four centimeters below the surface through a piece of flexible Tygon tubing into a graduated pipet. The minimum bore diameter was 0.3 cm and withdrawal flow rates were less than 0.5 mL per second; these procedures were adopted to minimize aggregate disruption.

## 5. Experimental Results and Discussion

The predicted size distributions for Brownian and shear coagulation were verified for kaolinite and illite clay particles sheared in artificial seawater. This section only summarizes the results which are presented in detail in Hunt (1980).

### Kaolinite

Because of larger aggregate breakup during counting, valid kaolinite aggregate size distributions were measured only for diameters from 0.6 to 1.2 μm. Figure 2 is an example of larger aggregate breakup during counting for one sample of kaolinite aggregates sized with 30, 70, and 140 μm diameter Coulter Counter apertures. The sample was withdrawn after 35 minutes of shearing at 4 $s^{-1}$. The settings of the Coulter Counter were chosen to measure the smallest aggregates possible with each aperture such that the counts recorded were always ten times greater than the counts recorded in a blank solution. The lack of alignment between apertures in their regions of overlap was caused by aggregate breakup during passage through the apertures where flow rates and fluid shear are high. The problem of larger aggregate breakup existed during all coagulation experiments with solid particles.

Kaolinite coagulation experiments were conducted at shear rates of 1, 2, 4, 8, 16, and 32$s^{-1}$. At each shear rate the reciprocal of the total suspended volumes, plotted in Figure 3, were linear with time as expected from Equation (4.10). The slopes of the lines, which are the second order removal rate constants, increased with shear rate to a maximum at 16 $s^{-1}$.

The volume removal rate declined at $G = 32\ s^{-1}$ because of a fluid instability. The volume flux through the distribution was estimated from Equation (4.11).

Volume distributions and normalized volume distributions are given in Figure 4 for a fluid shear rate of $1\ s^{-1}$. The volume distributions measured during the batch experiment had the same shape, only shifted downward with time. This local equilibrium in the size distribution indicates the assumption of a steady state size distribution made in the derivation was reasonable. Normalization of diameters and volume distributions reduced the vertical spread,and a line of slope 3/2, the Brownian prediction, fits the trend of the data. No region of possible shear coagulation dominance was observed because larger aggregates were broken up during the counting process.

Volume distributions measured over time at shear rates of 2, 4, 8, 16, and $32\ s^{-1}$ also achieved self-similar distributions which were reduced in spread on normalization. According to Equations (4.6) and (4.7), normalized volume distributions measured at all shear rates and volume fluxes should fall on a single curve. The agreement between the kaolinite data and the predictions was tested in Figure 5 where all normalized kaolinite data were plotted, excluding the larger aggregate data at each shear rate dominated by brea during counting. A line of slope 3/2, the Brownian prediction, fits the trend of the data for $\delta < 0.9$, and a level line, the shear prediction, fits the data for $\delta > 0.9$. The vertical spread in the normalized data present at each shear rate is caused by the overestimation of the volume flux from the total suspended volume removal rate. The dimensionless coagulation constants are estimated to be $A_b = 0.19$ and $A_{sh} = 0.15$.

## Illite

Experiments were conducted with illite in seawater at shear rates of 1/2, 1, 2, 4, 8, 16, and 32 $s^{-1}$. Inverse total suspended volumes during batch experiments are plotted in Figure 6 and the data indicate that the maximum removal rate constant occured at 8 $s^{-1}$. A fluid instability prevented the removal of suspended volume during the experiment at G = 32 $s^{-1}$.

Volume distributions measured during each illite experiment were self-similar in shape and the vertical spread was substantially reduced on normalization. Figure 7 is a plot of the normalized data for shear rates from 1/2 to 16 $s^{-1}$ including only that portion of the distributions not dominated by aggregate breakup during counting. In the plot a line of slope 3/2 and a level line were drawn by eye and fit the trend of the data. The vertical spread in the normalized data is less than that observed for kaolinite, and unlike kaolinite, the separation between Brownian and shear coagulation dominance occurs at about $\delta = 0.44$. The normalized data for G = 16 $s^{-1}$ are above the trend of the other data and combined with the decreased volume removal rate shown in Figure 6, indicate that aggregate breakup in the rotating cylinder apparatus was occurring at this shear rate. At G = 32 $s^{-1}$ the volume distributions could not be normalized because there was no decrease in total suspended volume. The dimensionless constants characterizing illite coagulation in seawater were $A_b = 0.4$ and $A_{sh} = 0.12$.

## Discussion

This discussion compares the assumptions necessary in the derivation of coagulating and settling particle size distributions with the experimental results for clay particles in artificial seawater.

The first assumption, and most drastic in terms of departure from previous coagulation research, was the existence of a particle size distribution in local equilibrium, maintained by a flux of particle mass through the size distribution. Experimentally, a constant flux of small particles into the distribution could not be imposed while maintaining a known rate of laminar fluid shear. Instead, batch experiments were conducted and decaying self-similar particle size distributions were observed. The second assumption required the dominance of only one coagulation or settling mechanism at a given size. Experimental results indicate the assumption is reasonable for Brownian and shear coagulation. A transition region between the mechanisms exists and is probably less than a factor of two in diameter. The dominant contribution to the mass flux through the size distribution appears to be determined by collisions between particles comparable in size.

The concentration of ions in artificial seawater was sufficient to destabilize kaolinite and illite clay particles. The greater surface charge of illite particles caused illite aggregates to be more porous than kaolinite aggregates. This difference in aggregate porosity is a reasonable basis to explain qualitatively the different results for kaolinite and illite (Hunt, 1980). For kaolinite the normalized diameter separating

Brownian and shear coagulation occurred at $\delta = 0.9$, while for illite the separation was at $\delta = 0.44$. The dimensionless coagulation constants for kaolinite and illite were different along with the volume removal rate constant at a given shear rate. Finally, illite aggregates were more susceptible to aggregate breakup at higher fluid shear rates.

The last assumption was that coagulation and sedimentation mechanisms could be represented by characteristic parameters of the mechanisms. The choice of $\rho_p^{-1}G$ to characterize shear coagulation was shown to be valid, and the choice of $kT/\mu$ for Brownian coagulation appears to be reasonable, although experiments were conducted only at room temperature. In the specification of particle mass flux through the distribution and identification of characteristic parameters for coagulation and settling, aggregate density was implicitly assumed to be independent of particle size. For the experimental data collected over the narrow range of 0.6 to about 1.2 μm, equivalent spherical diameter, the assumption of uniform aggregate density is probably reasonable. Experimental evidence indicates that aggregate density decreases with increasing aggregate diameter over the range 1 to 2000 μm (McCave, 1975; Tambo and Watanabe, 1979).

Preliminary experiments were conducted with dilute oil-in-water emulsions to avoid the problems of aggregate breakup during counting and aggregate density variations with size. For simple oil-in-water emulsions, mechanically dispersed in high ionic strength solutions, the oil droplets were not completely destabilized, and the results could not be used for testing the coagulation and settling size distribution predictions (Hunt, 1980).

## 5. Conclusions

Predictions of coagulating and settling particle size distributions were obtained by dimensional analysis, following techniques developed for analysis of aerosol dynamics and small-scale velocity and scalar fluctuations in turbulent fluids. Considerable simplification of coagulation and settling mechanisms was necessary and the predictions apply only after a local equilibrium has developed in the size distribution. The predicted size distributions for Brownian and shear coagulation were verified with clay particles destabilized in artifical seawater. Measured particle size distributions were in agreement with the predicted dependence on diameter, fluid shear rate, and particle volume flux through the distribution. Because larger aggregates could not be sized, predictions for differential sedimentation coagulation and settling were not tested.

The dimensional analysis approach is a simple and quantitative technique for describing coagulation and settling in continuous particle size distributions. Only a single dimensionless constant is required to characterize each coagulation or settling mechanism. The experimental results for kaolinite and illite clays indicate that the dimensionless constants are a function of particle surface chemistry and probably a function of the ionic composition of the destabilizing solution. At this time the dimensionless constants must be determined experimentally, but once obtained, they allow a far more convenient analysis of coagulation and settling, after sufficient time, than a formal solution to Equation (1.3).

The verified predictions for Brownian and shear coagulation of clay particles have direct application to clay particle removal from seawater. The results have possible application to other natural waters and particle separation processes, where information is required on particle size distributions and total suspended volume removal rates. A number of important particle-fluid interactions were not considered, including aggregate breakup by fluid shear and coagulation in turbulent fluids containing a distribution of local shear rates. The understanding of coagulation gained in the work provides a theoretical and experimental framework for considering other mechanisms and flow regimes.

Acknowledgement

The author thanks the following organizations for their financial support of this work: United States Environmental Protection Agency, Union Oil Company, Jessie Smith Noyes Foundation, Inc., and United States National Oceanographic and Atmospheric Administration, Office of Sea Grant. The work presented here is from material submitted in a doctorial thesis by the author to the California Institute of Technology, Pasadena, California. During the course of this research the author received helpful advice from James J. Morgan and E. John List.

Appendix

The predicted particle size distributions for Brownian, shear, and differential sedimentation coagulation and gravitational settling are integrated to obtain expressions for the total suspended volume during batch experiments.

The total suspended volume at time t is given by

$$V(t) = \int_0^\infty \frac{\pi}{6} d_p^3 \, n(d_p,t) \, d(d_p) \qquad (A.1)$$

noting explicitly the time dependence of the size distribution. Predictions for Brownian, shear, and differential sedimentation coagulation are substituted into Equation (A.1) and the regions of dominance for each mechanism are obtained by assuming continuity between predictions and solving for the diameter of intersection. The predicted size distributions and regions of dominance are

Brownian

$$n(d_p,t) = A_b \left(\frac{E(t)}{K}\right)^{1/2} d_p^{-5/2}, \quad 0 < d_p \leq \left(\frac{K A_{sh}^2}{G A_b^2}\right)^{1/3} \qquad (A.2)$$

shear

$$n(d_p,t) = A_{sh} \left(\frac{E(t)}{G}\right)^{1/2} d_p^{-4}, \quad \left(\frac{K A_{sh}^2}{G A_b^2}\right)^{1/3} < d_p \leq \frac{G A_{ds}^2}{S A_{sh}^2} \qquad (A.3)$$

differential sedimentation

$$n(d_p,t) = A_{ds} \left(\frac{E(t)}{G}\right)^{1/2} d_p^{-9/2}, \quad \frac{G\, A_{ds}^2}{S\, A_{sh}^2} < d_p < \infty. \tag{A.4}$$

Since a local equilibrium in the size distributions exists, only the volume flux is time dependent. The fluid shear rate is assumed to be large enough for a shear-dominated region to exist, that is, $G > K^{1/4}\, S^{3/4}\, A_{sh}^2 / A_b^{1/2}\, A_{ds}^{3/2}$.

On substituting Equations (A.2), (A.3), and (A.4) into Equation (A.1) and integrating, obtain

$$V(t) = \alpha \left(\frac{E(t)}{G}\right)^{1/2} \tag{A.5}$$

where $\alpha$ is defined as

$$\alpha = \pi A_{sh} \left[\frac{4}{9} + \frac{1}{6} \ln \frac{G^{4/3}\, A_b^{2/3}\, A_{ds}^2}{K^{1/3}\, S\, A_{sh}^{8/3}}\right] \tag{A.6}$$

and an expression for E(t) is obtained from Equation (A.5)

$$E(t) = \frac{G}{\alpha^2} V^2(t) \quad . \tag{A.7}$$

Substituting in the approximate relationship between volume flux and rate of change of suspended volume from Equation (4.8) have

$$\frac{dV(t)}{dt} \approx - \frac{G}{\alpha^2} V^2(t) \tag{A.8}$$

with a solution of

$$V(t) \approx \frac{1}{V_0^{-1} + \frac{G}{\alpha^2}\, t} \tag{A.9}$$

where $V_0$ is the total suspended volume at $t = 0$.

The derivation of Equation (A.9) assumed the size distribution was composed of regions dominated by Brownian, shear, and differential sedimentation coagulation and neglected gravitational settling. A result similar to Equation (A.9) is derived for a size distribution dominated by Brownian and shear coagulation and gravitational settling, noting that the particle diameter separating shear coagulation and settling is $G^{2/3}\, S^{-1}\, E^{1/3}\, (A_s/A_{sh})^{4/3}$. Following the analysis above gives

$$V(t) = \left(\frac{E(t)}{G}\right)^{1/2} \pi A_{sh} \left[\frac{1}{3} + \frac{1}{6}\, \ell n\, \frac{G\, E^{1/3}\, A_b^{2/3}\, A_s^{4/3}}{K^{1/3}\, S\, A_{sh}^{2}}\right] \tag{A.10}$$

and assuming that the $\ell n\, E^{1/3}$ term in the bracket has small variation over time, a parameter $\alpha'$ is defined as

$$\alpha' = \pi A_{sh} \left[\frac{1}{3} + \frac{1}{6}\, \ell n\, \frac{G\, E^{1/3}\, A_b^{2/3}\, A_s^{4/3}}{K^{1/3}\, S\, A_{sh}^{2}}\right] \tag{A.11}$$

As above, obtain

$$V(t) \approx \frac{1}{V_0^{-1} + \frac{G}{\alpha'^2}\, t} \tag{A.12}$$

as the approximate variation in total suspended volume over time for dominance by Brownian and shear coagulation and gravitational settling.

Both Equations (A.9) and (A.12) predict that a plot of inverse total suspended volume should be approximately linear with time with a slope dependent upon the shear rate.

References


Batchelor, G. K. 1953. The Theory of Homogeneous Turbulence. Cambridge University Press.

Batchelor, G. K. 1959. Small-scale variation of convected quantities like temperature in turbulent fluid, part 1. General discussion and the case of small conductivity. J. Fluid Mech. 5, 113-133.

Birkner, F. B. and Morgan, J. J. 1968. Polymer flocculation kinetics of dilute colloidal suspensions. J. Amer. Water Works Assoc. 60, 175-191.

Drake, R. L. 1976. Similarity solutions for homogeneous and nonhomogeneous aerosol balance equations. J. Colloid Interface Sci. 57, 411-423.

Edzwald, J. K., Upchurch, J. B. and O'Melia, C. R. 1974. Coagulation in estuaries. Environ. Sci. Technol. 8, 58-63.

Friedlander, S. K. 1960a. On the particle-size spectrum of atmospheric aerosols. J. Meteorol. 17, 373-374.

Friedlander, S. K. 1960b. Similarity considerations for the particle-size spectrum of a coagulating, sedimenting aerosol. J. Meteorol. 17, 479-483.

Friedlander, S. K. 1977. Smoke, Dust and Haze: Fundamentals of Aerosol Behavior. Wiley-Interscience.

Gelbard, F. and Seinfeld, J. H. 1979. The general dynamic equation for aerosols, theory and application to aerosol formation and growth. J. Colloid Interface Sci., 68, 363-382.

Honig, E. P., Roebersen, G. J. and Wiersema, P. H. 1971. Effect of hydrodynamic interaction on the coagulation rate of hydrophobic colloids. J. Colloid Interface Sci., 36, 97-109.

Hunt, J. R. 1980. Coagulation in continuous particle size distributions; theory and experimental verification. Ph.D. thesis, California Institute of Technology, Pasadena.

Hunt, J. R., in press. Prediction of oceanic particle size distributions from coagulation and sedimentation mechanisms. Advances in Chemistry Series 189.

Kerr, P. F. et al. 1949-50. Reference Clay Minerals; American Petroleum Institute Research Project 49. Preliminary Reports No. 1-8. Columbia University.

Lawler, D. F., O'Melia, C. R. and Tobiason, J. E., in press. Integral water treatment plant design: from particle size to plant performance. Advances in Chemistry Series 189.

Lichtenbelt, J. W. Th., Pathmamanotharan, C. and Wiersema, P. H. 1974. Rapid coagulation of polystyrene latex in a stopped-flow spectrophotometer. J. Colloid Interface Sci., 49, 281-285.

Manley, R. St. J. and Mason, S. G. 1955. Particle motions in sheared suspensions III. Further observations on collisions of spheres. Can. J. Chem. 33, 763-773.

Mason, B. J. 1971. Physics of Clouds, 2nd ed. Clarendon Press.

McCave, I. N. 1975. Vertical flux of particles in the ocean. Deep-Sea Res. 22, 491-502.

Overbeek, J. Th. G. 1977. Recent developments in understanding of colloid stability. J. Colloid Interface Sci. 58., 408-422.

Pulvermacher, B. and Ruckenstein, E. 1974. Similarity solutions of population balances. J. Colloid Interface Sci. 46, 428-436.

Riley, J. P. and Skirrow, G. 1965. Chemical Oceanography, Vol. 1, Academic Press.

Smoluchowski, M. 1917. Versuch einer Mathematischen Theorie der Koagulationkinetik Kolloider Lösungen (Trial of a mathematical theory of the coagulation kinetics of colloidal solutions). Z. Physik. Chem. 92, 129-168.

Spielman, L. A. 1970. Viscous interactions in Brownian coagulation. J. Colloid Interface Sci. 33, 562-571.

Spielman, L. A. 1977. Particle capture from low-speed laminar flows. Ann. Rev. Fluid Mech. 9, 297-319.

Swift, D. L. and Friedlander, S. K. 1964. The coagulation of hydrosols by Brownian motion and laminar shear flow. J. Colloid Sci. 19, 621-647.

Tambo, N. and Watanabe, Y. 1979. Physical characteristics of flocs - I. The floc density function and aluminum floc. Water Res. 13, 409-419.

Taylor, G. I. 1936. Fluid friction between rotating cylinders Part I. Torque measurements. Proc. Royal Soc. A 157, 546-564.

van de Ven, T. G. M. and Mason, S. G. 1977. The microheology of colloidal dispersions VII. Orthokinetic doublet formation of spheres. Colloid Polym. Sci. 255, 468-479.

van Olphen, H. 1977. An Introduction to Clay Colloid Chemistry, 2nd ed. Wiley-Interscience.

Wang, C. S. and Friedlander, S. K. 1967. The self-preserving particle size distribution for coagulation by Brownian motion II. Small particle slip correction and simultaneous shear flow. J. Colloid Interface Sci. 24, 170-179.

Zeichner, G. R. and Schowalter, W. R. 1977. Use of trajectory analysis to study stability of colloidal dispersions in flow fields. AIChE, 23(3), 243-254.

Figure 1 Comparison of Brownian, shear, and differential sedimentation coagulation collision functions for particles of diameter $d_p$ colliding with particles of diameter $\frac{1}{2} d_p$; assuming T = 25°C, G = 10 $s^{-1}$, and $(\rho_p - \rho_f)$ = 0.1 g $cm^{-3}$.

Figure 2 Volume distributions of kaolinite after 35 minutes of shearing at G = 4 $s^{-1}$ measured by 30, 70, and 140 μm apertures.

Figure 3 Inverse total suspended particle volume during kaolinite experiments at shear rates of 1, 2, 4, 8, 16, and 32 $s^{-1}$.

Figure 4 Volume distributions and normalized volume distributions for kaolinite at G = 1 $s^{-1}$.

Figure 5 Normalized distributions for kaolinite at G = 1, 2, 4, 8, 16, and 32 $s^{-1}$.

Figure 6 Inverse total suspended particle volume during illite experiments at shear rates of 1/2, 1, 2, 4, 8, 16, and 32 $s^{-1}$.

Figure 7 Normalized volume distributions for illite at G = 1/2, 1, 2, 4, 8, and 16 $s^{-1}$.

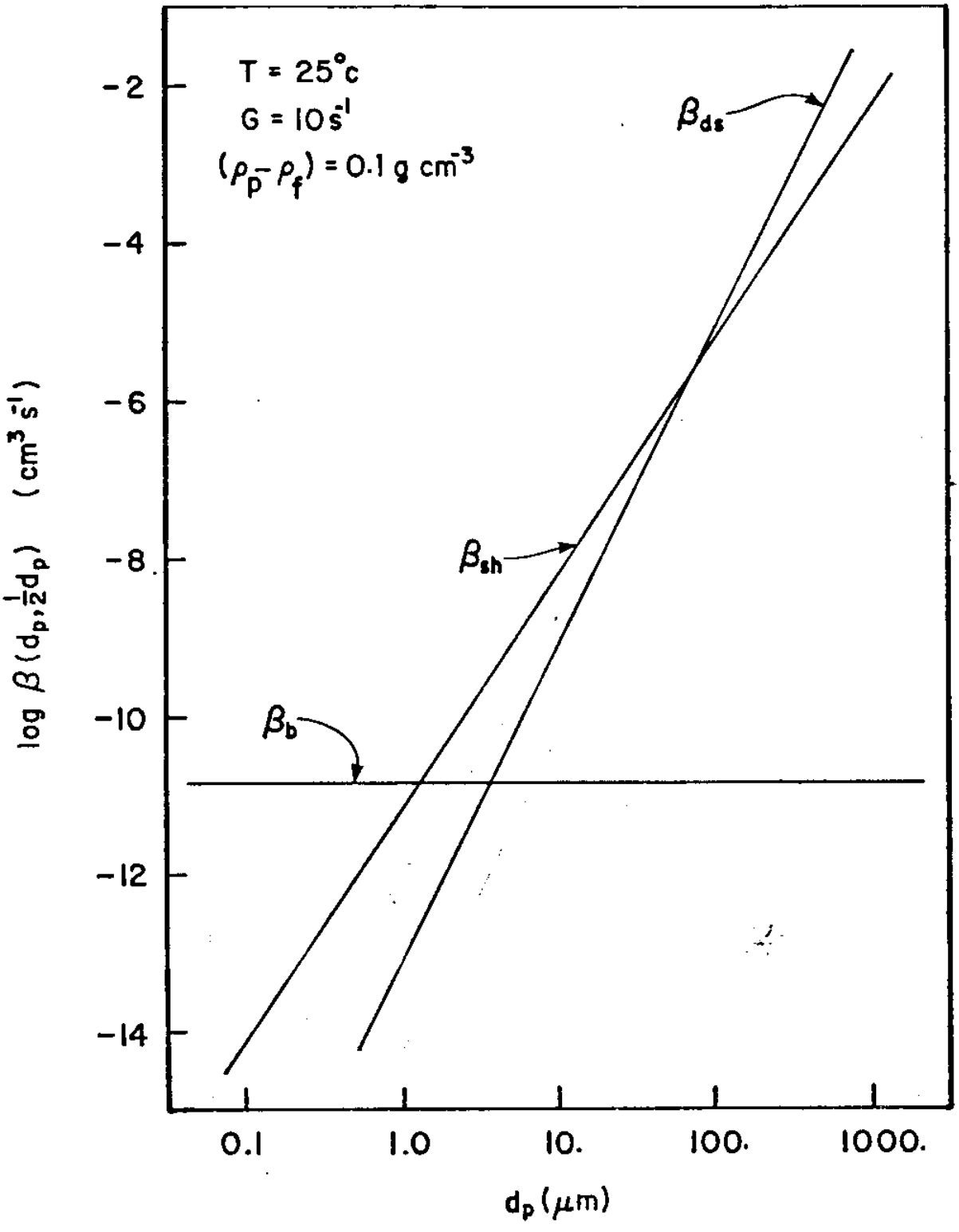
T = 25°c
G = 10 s⁻¹
(ρp − ρf) = 0.1 g cm⁻³
βds
βsh
βb
-2
-4
-6
-8
-10
-12
-14
log β(dp, ½dp) (cm³ s⁻¹)
0.1
1.0
10.
100.
1000.
dp (μm)

Figure 1

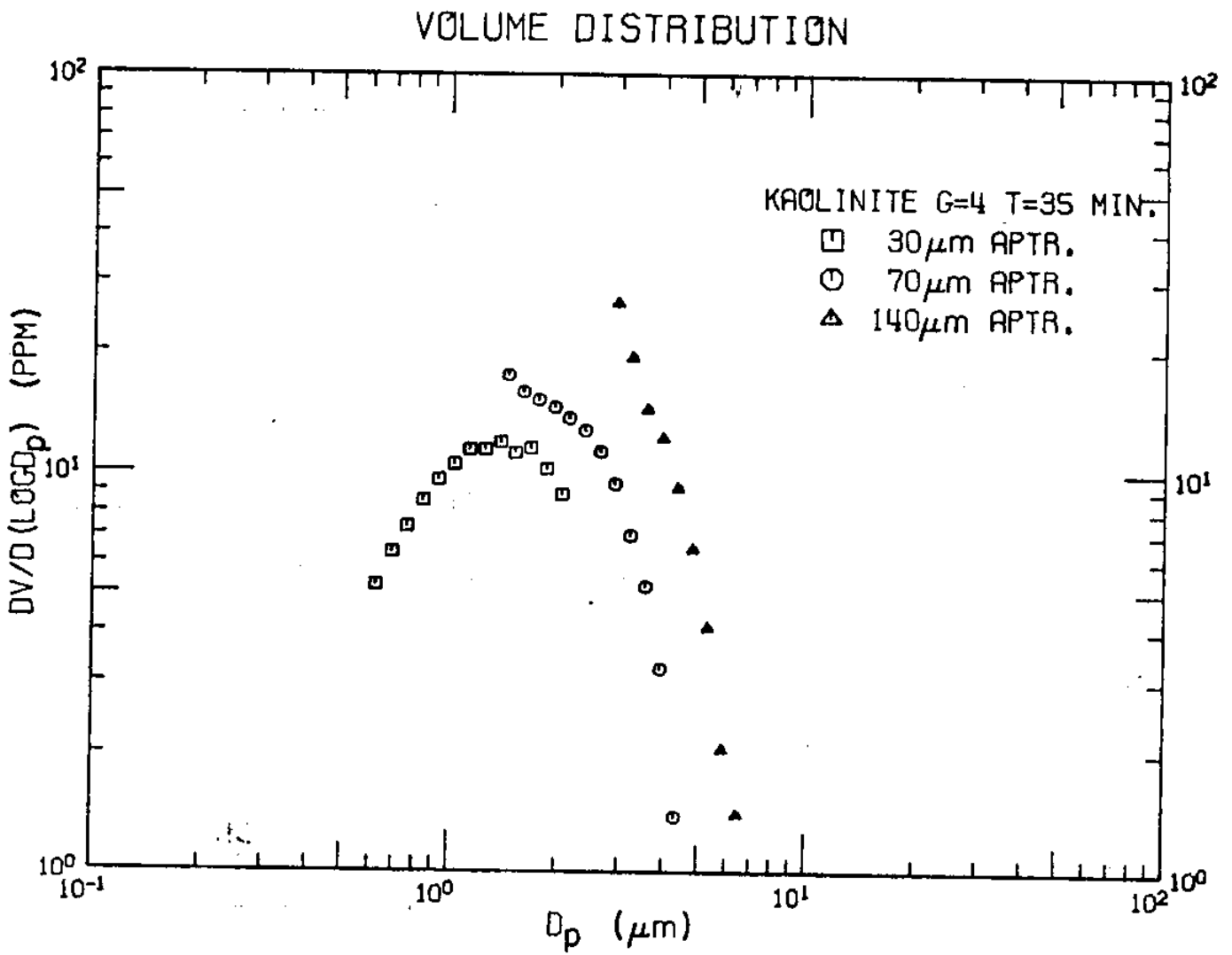
VOLUME DISTRIBUTION
KAOLINITE G=4 T=35 MIN.
30μm APTR.
70μm APTR.
140μm APTR.
DV/D(LOGDp) (PPM)
Dp (μm)
10²
10¹
10⁰
10⁻¹
10⁰
10¹
10²

Figure 2

CHANGES IN INVERSE TOTAL KAOLINITE VOLUME OVER TIME FOR VARIOUS SHEAR RATES

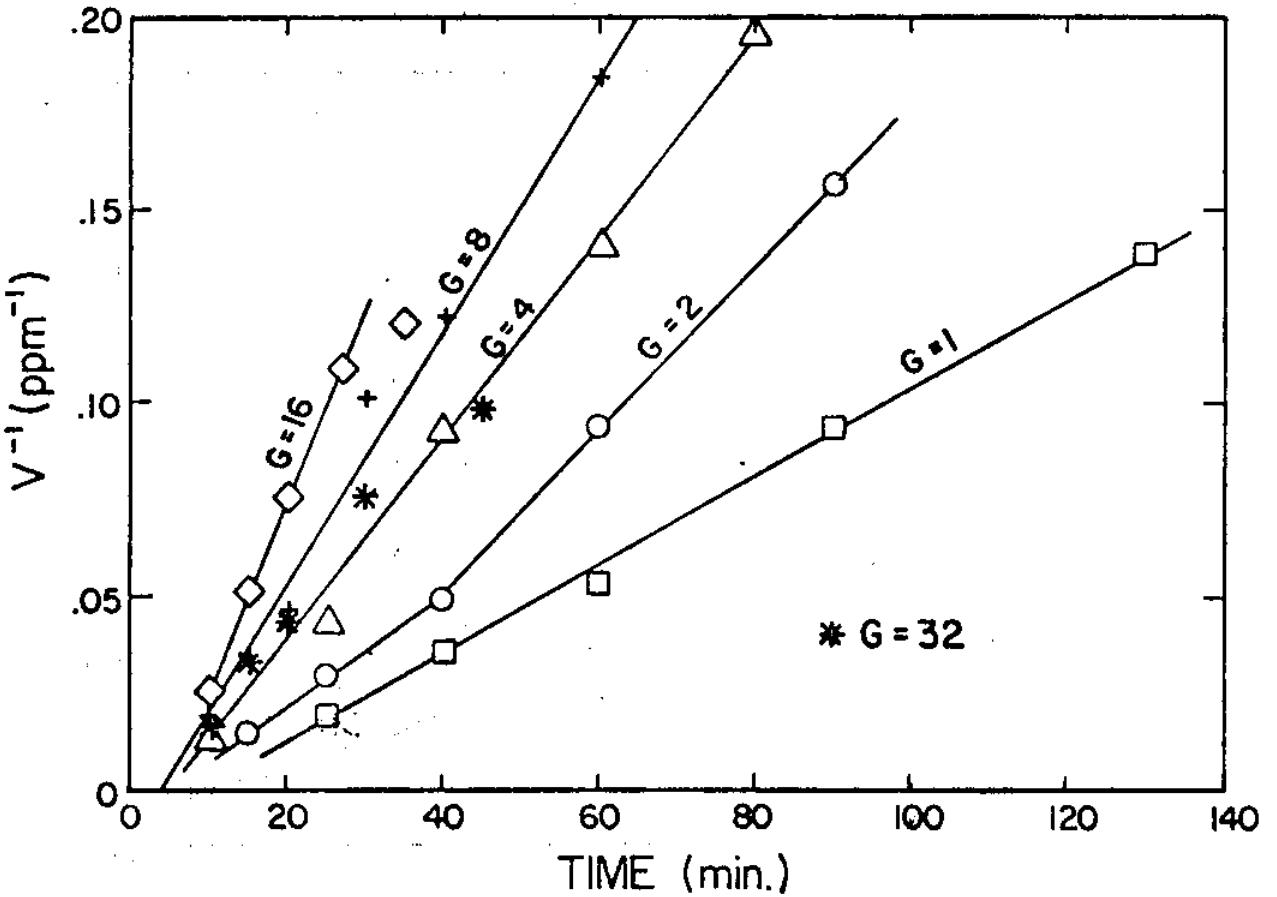

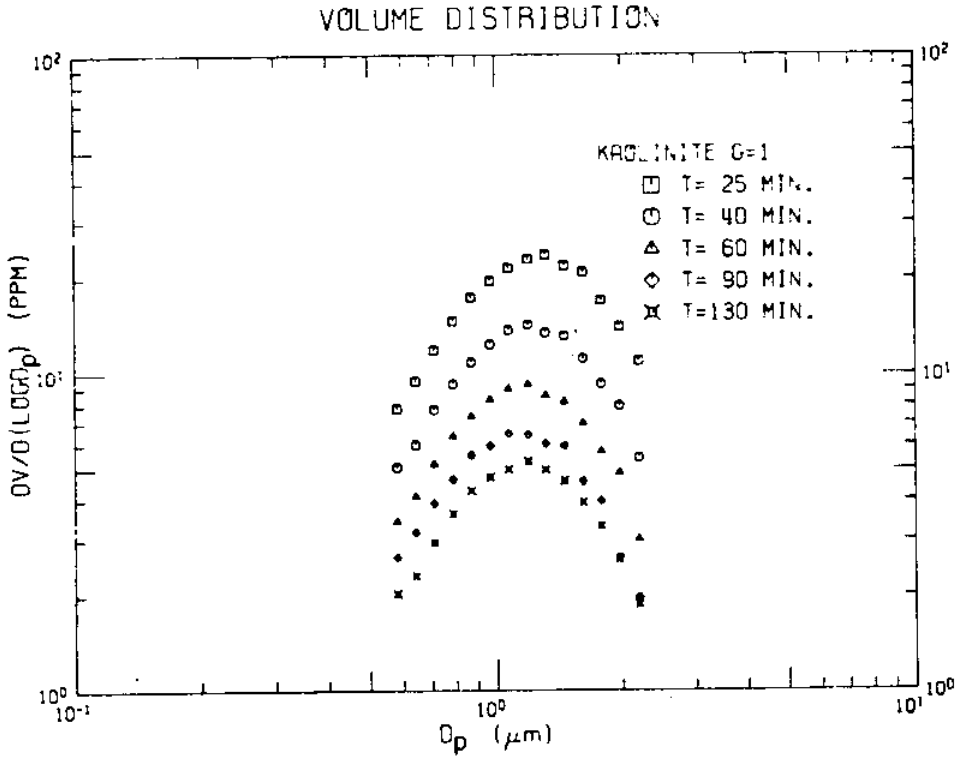
VOLUME DISTRIBUTION
KAOLINITE G=1
T= 25 MIN.
T= 40 MIN.
T= 60 MIN.
T= 90 MIN.
T=130 MIN.
ΔV/D(LOGDp) (PPM)
Dp (μm)

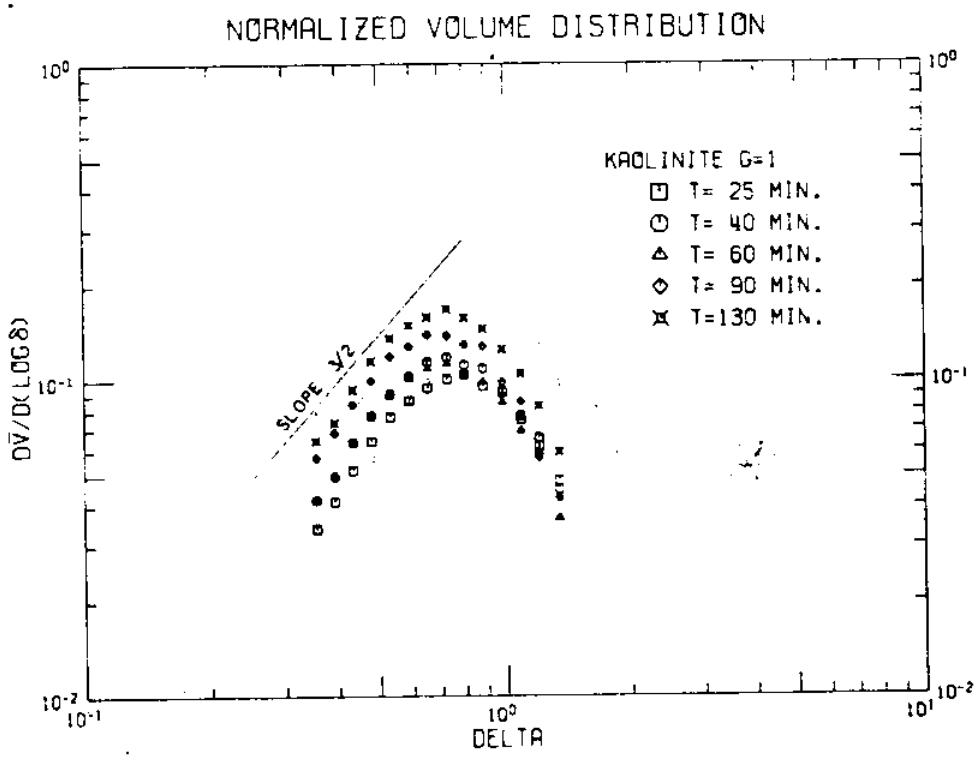
NORMALIZED VOLUME DISTRIBUTION
KAOLINITE G=1
T= 25 MIN.
T= 40 MIN.
T= 60 MIN.
T= 90 MIN.
T=130 MIN.
SLOPE -1/2
ΔV̄/D(LOGδ)
DELTA

Figure 4

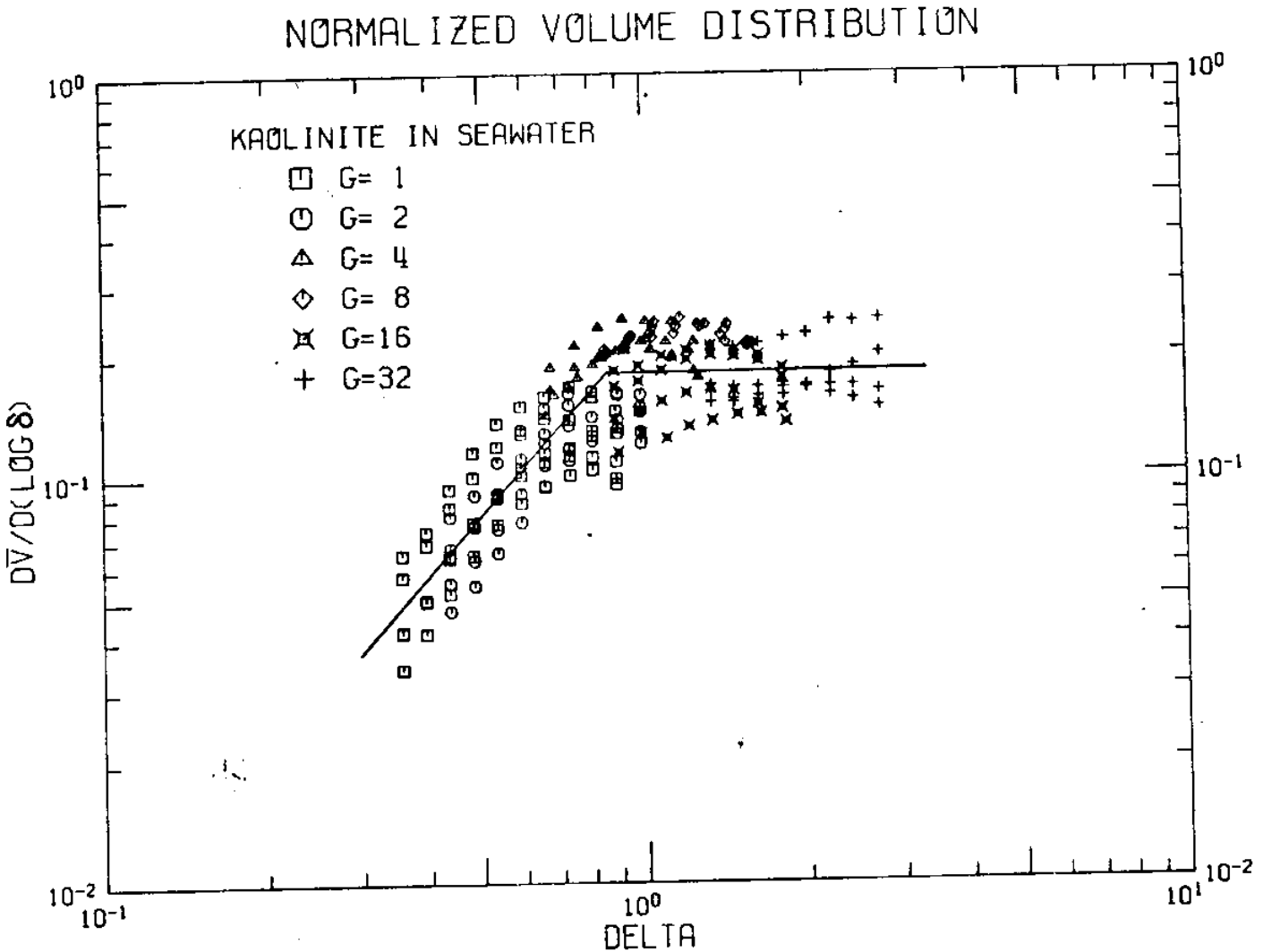
NORMALIZED VOLUME DISTRIBUTION
KAOLINITE IN SEAWATER
G= 1
G= 2
G= 4
G= 8
G=16
G=32
DV/D(LOG δ)
DELTA
10^0
10^-1
10^-2
10^1

Fig 5

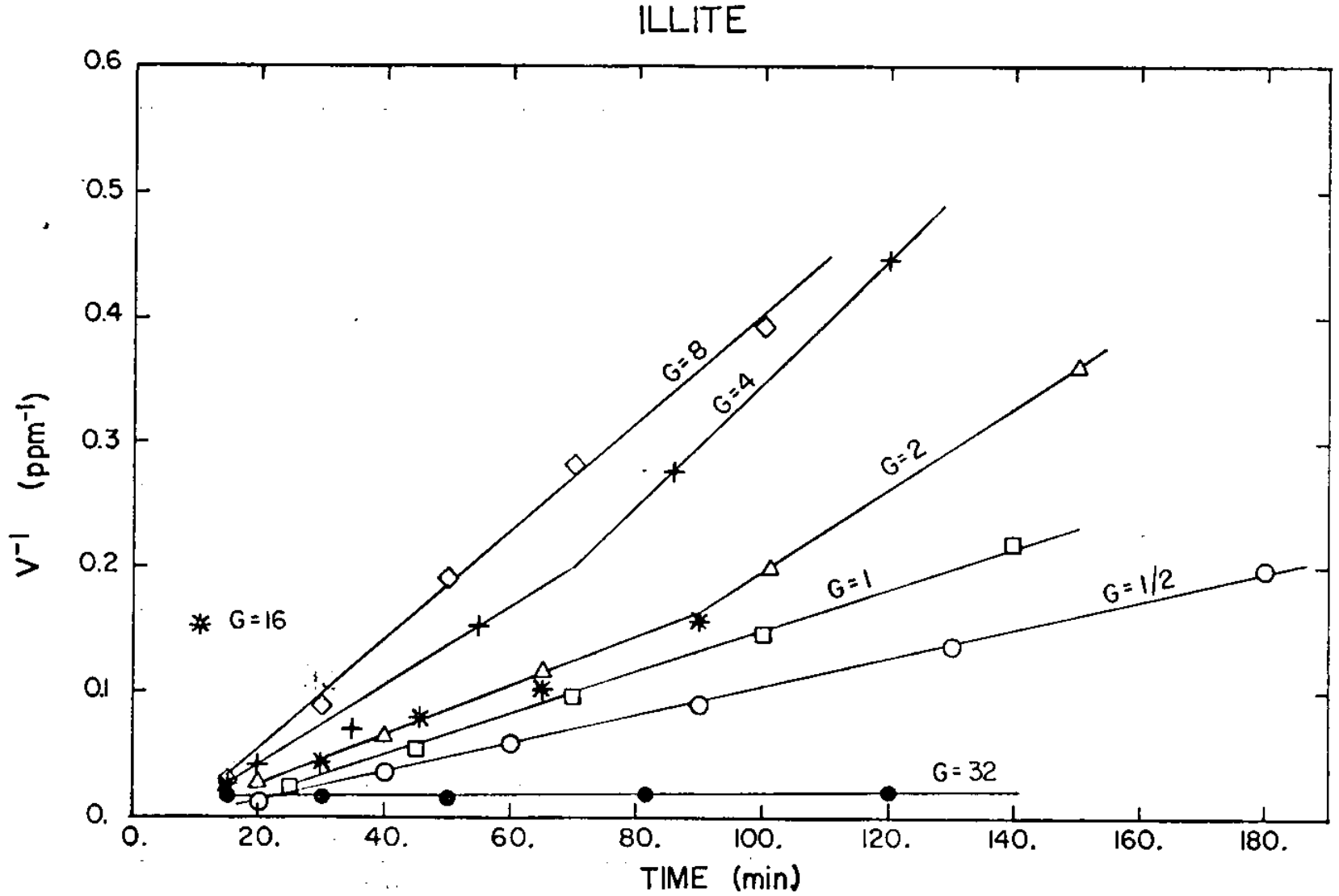
ILLITE
0.6
0.5
0.4
0.3
0.2
0.1
0.
V⁻¹ (ppm⁻¹)
G=8
G=4
G=2
G=1
G=1/2
G=16
G=32
0.
20.
40.
60.
80.
100.
120.
140.
160.
180.
TIME (min)

Fig. 6

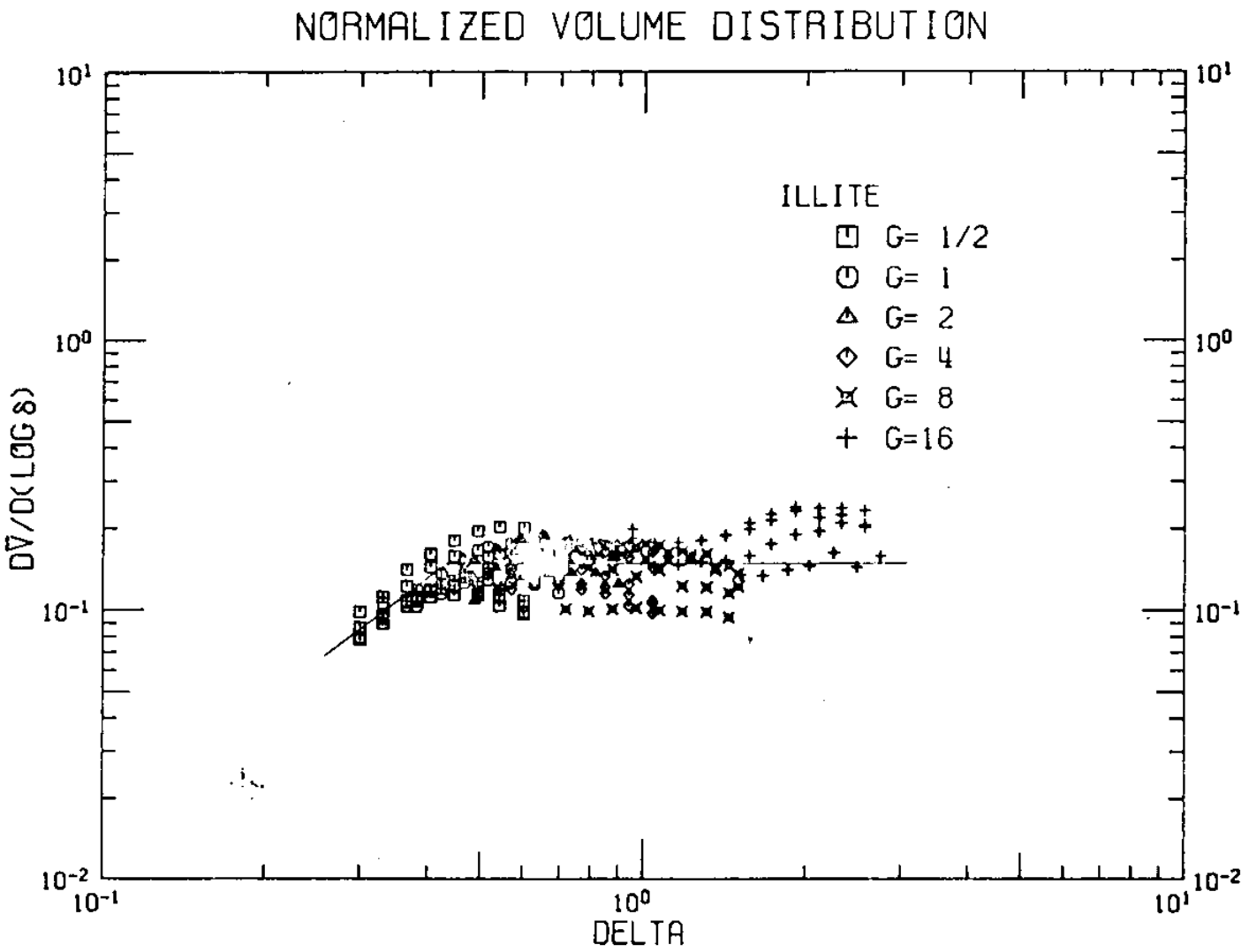
NORMALIZED VOLUME DISTRIBUTION
ILLITE
G= 1/2
G= 1
G= 2
G= 4
G= 8
G=16
DV/D(LOG δ)
DELTA
10¹
10⁰
10⁻¹
10⁻²

Fig. 7